Journal of Zhejiang University-SCIENCE A (Applied Physics & Engineering) 2025 26(6):573-584
www.jzus.zju.edu.cn; www.springer.com/journal/11582
E-mail: jzus_a@zju.edu.cn

Regular paper

https://doi.org/10.1631/jzus.A2400148

Centrifuge modeling of contaminant transport in keyed sand-bentonite cutoff walls

Bo HUANG, Linfeng CAO, Jiachen GUO, Chunrui XU, Yuchao LI✉

MOE Key Laboratory of Soft Soils and Geoenvironmental Engineering, Department of Civil Engineering, Zhejiang University, Hangzhou 310058, China

Abstract: Sand-bentonite (SB) cutoff walls are commonly used as barriers in polluted areas. The embedded part of an SB wall in an aquitard is crucial for its performance. In this study, a centrifuge modeling test was carried out to investigate the effect of contact between the key and the aquitard on the migration behavior of contaminants within an SB cutoff wall. The centrifuge was accelerated to 100*g* (gravitational acceleration) and maintained in-flight for 36 h, equivalent to 41 years of transport time in the prototype. Results showed that the contaminant concentration within the SB wall was higher downstream than in the middle in the thickness direction, and deeper regions exhibited a greater concentration than shallower ones. This concentration distribution indicated that contaminants were transported along the interface between the SB wall and the aquitard, bypassing the base of the SB wall to reach the downstream aquifer rapidly. An improved numerical simulation considering preferential interface migration was performed, which agreed with the centrifuge test results. The simulation results indicated that preferential interface migration, as a defect, significantly accelerated the speed of contaminant migration, reducing the breakthrough time of the SB wall to 1/9 of that without preferential interface migration.

Key words: Cutoff wall; Centrifuge modeling; Contaminant transport; Defect; Breakthrough time

1 Introduction

Sand-bentonite (SB) vertical cutoff walls are widely used in underground barrier isolation measures to prevent or delay contaminants from leaving the site (Ruffing et al., 2018; Cao et al., 2021; Wei et al., 2023). Typically, a trench measuring 0.6–1.2 m wide is excavated along the perimeter of a contaminated site and then filled with a mixture of in-situ deposits and bentonite slurry to form a flexible wall (D'Appolonia, 1980; Li et al., 2015). To reduce leakage, SB walls are usually embedded in an aquitard, like a rock or clay layer, in which the embedded part of the SB wall is called the "key". The key's performance significantly influences the service life of an SB wall (Tachavises and Benson, 1997; Lee and Benson, 2000). The design life of an SB wall in geoenvironmental control projects is typically around 30 years or even longer, as some organic contaminants have attenuation half-lives longer than 30 years (Ruffing et al., 2018). However, when a defect occurs in the key, the service life of the SB wall falls far short of its design value. Therefore, it is useful to investigate the impact of the key on contaminant transport for predicting the service life of SB walls in geoenvironmental projects.

Due to the cost and duration of field studies, few field surveys have reported observational data regarding pollutant transport in SB walls in treated contaminate sites (Ryan et al., 2022), and only few researchers have investigated the distribution of effective stress on the walls (Ryan and Spaulding, 2008; Tong et al., 2020). In laboratory studies, Lee and Benson (2000) prepared a scale model of a sandy deposit with an SB wall. They studied the influence of defects on the impermeability of the SB wall and revealed the importance of keys. However, the stress levels they tested were lower than actual, which resulted in unrealistic parameters of the SB wall or the contact state with the surrounding soil and did not simulate the transport of

✉ Yuchao LI, liyuchao@zju.edu.cn
Bo HUANG, https://orcid.org/0000-0002-7293-8618
Linfeng CAO, https://orcid.org/0000-0001-8211-7445

Received Mar. 14, 2024; Revision accepted June 28, 2024; Crosschecked Apr. 15, 2025

pollutants. In contrast, geotechnical centrifuge modeling tests have advantages. First, they achieve a stress level similar to that of a prototype, allowing for an accurate simulation of the parameters of the SB wall and the contact state between the SB wall and its surrounding soil. Second, centrifuge tests accelerate the transport of contaminants, making them potentially feasible for simulating long-term contaminant transport.

Previous studies have successfully modelled the migration of various pollutants in layered liners using centrifuge tests (Arulanandan et al., 1988; Knight and Mitchell, 1996; Gamerdinger et al., 2001; Hutchison et al., 2003; Soga et al., 2003; Lo et al., 2005; Timms et al., 2009; Kumar and Singh, 2012; Shu et al., 2018). However, few studies have investigated the migration of pollutants in vertical barriers using centrifuge tests. Kererat et al. (2013) conducted four experiments under the condition of 30*g* (gravitational acceleration) to study the migration of light non-aqueous phase liquids (LNAPLs) in sandy sites featuring a hanging soil-cement cutoff wall. Zhan et al. (2023a) performed a centrifuge experiment (100*g*) for 43.8 h to compare the long-term performance of loess-modified and unmodified SB walls. However, both sides of the cutoff wall were rigid porous stones instead of aquifers, which resulted in inconsistent stress between the experimental model and the field. The stress state significantly affects the contaminant transport parameters of SB walls, including their porosity and hydraulic conductivity (Filz et al., 2001; Yeo et al., 2005). In addition, the bottom of the SB walls was not embedded with an aquitard but sealed with metal slots, overlooking the influence of the key on the performance of SB walls (Tachavises and Benson, 1997; Lee and Benson, 2000). Hence, integrating the deposits surrounding an SB wall (aquifer and aquitard) into a scaled model could offer a more realistic method to emulate the working conditions of vertical barriers.

The objective of this paper is to present the results of centrifuge tests of chloride ion (Cl^-) migration in sandy sites featuring a keyed SB cutoff wall, and investigate the impact of the key on the migration of contaminants. Additionally, the similitude of the horizontal effective stress of the SB wall is discussed. Finally, numerical analysis was conducted by applying the finite-element (FE) method, through which the migration behavior and breakthrough time in the SB wall were computed.

2 Centrifuge modeling

2.1 Scaling laws

To evaluate the similitude of the contaminant transport process in the centrifuge modeling test, Arulanandan et al. (1988) proposed eight dimensionless numbers and discussed the conditions for their similitude (Table 1). When the experiment uses the same soil and contaminant solution as the prototype and the adsorption meets equilibrium adsorption, the dimensionless numbers π_1, π_3, π_4, π_5, and π_6 are identical in the model and its prototype, but π_2 (Reynolds number), π_7 (dynamic effect), and π_8 (Péclet number) are not identical. Note that although the expressions of π_2 and π_8 are the same as the Reynolds and Péclet numbers, respectively, they have different physical meanings in the study of similarity in pollutant transport during centrifuge testing. The π_2 represents the dynamic similarity of fluid motion (Hensley and Schofield, 1991; Zhan et al., 2023a), created in a laminar scenario (π_2<1, to keep the validity of Darcy's law). The π_8 describes the relationship between the two dispersive phenomena of mechanical dispersion and molecular diffusion (Arulanandan et al., 1988; Cooke and Mitchell, 1991). When contaminant dispersion is dominated by the process of molecular diffusion (π_8<1), the dispersion can be modelled even without ensuring the similarity of π_8. The π_7 would be considered if dynamic events occurred.

Table 1 Summary of dimensionless numbers (Arulanandan et al., 1988)

Number	Formula	Commentary
Concentration	$\pi_1 = C/\rho_f$	Satisfied
Reynolds	$\pi_2 = \rho_f v_s l_p/\mu$	π_2<1, to keep the validity of Darcy's law
Advection	$\pi_3 = v_s t/l$	Satisfied
Diffusion	$\pi_4 = D_m t/l^2$	Satisfied
Capillary	$\pi_5 = \rho_f g l l_p/T_f$	Satisfied
Adsorption	$\pi_6 = S/\rho_f$	Equilibrium adsorption
Dynamic effect	$\pi_7 = gt^2/l$	Laminar flow
Péclet	$\pi_8 = v_s l_p/D_m$	π_8<1, to insure similarity in model and prototype

C is the concentration of contaminant in the pore water [ML^{-3}]; ρ_f is the fluid density [ML^{-3}]; v_s is the interstitial flow velocity [LT^{-1}]; l_p is the characteristic microscopic length (e.g., particle size) [L]; μ is the dynamic viscosity of the fluid [$ML^{-1}T^{-1}$]; t is the time [T]; l is the characteristic macroscopic length (e.g., sample height) [L]; D_m is the aqueous molecular diffusion coefficient in porous medium [L^2T^{-1}]; g is the gravitational acceleration [LT^{-2}]; T_f is the surface tension of the fluid particle interface [MT^{-2}]; S is the mass of the adsorbed contaminant per unit volume [ML^{-3}]

In this study, the similarity of π_1, π_3, and π_4 was achieved unconditionally, while π_5, π_6, and π_7 were not relevant to this study and therefore could be ignored. The similitude of π_2 and π_8 will be discussed further in Section 4.

2.2 Experimental facilities and model configuration

In this study, the ZJU-400 centrifuge from Zhejiang University, China was utilized. The centrifuge model was conceptualized based on a landfill located in China. This landfill, situated in a valley, was underlain by unweathered rock that acted as a relatively impermeable layer. An SB wall was installed downstream of the landfill. The model was placed in a strongbox measuring 770 mm×400 mm×510 mm (length×width×height), which was divided into three sections using two 8 mm-thick perforated baffles made of acrylic. The two end sections of the strongbox were designated as water reservoirs, while the middle section housed the SB wall and the surrounding soil deposits. The schematic setup of the model is shown in Fig. 1.

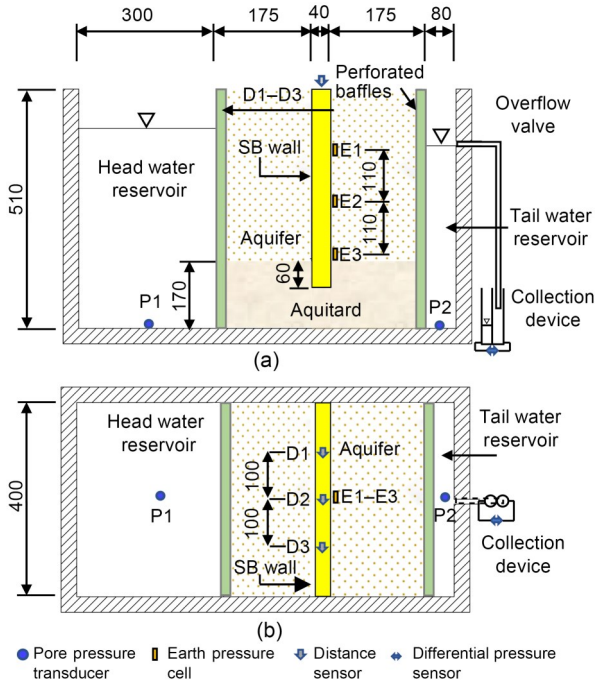

Fig. 1 Schematic diagram of the centrifuge model set-up (mm): (a) profile view; (b) plan view

The head water reservoir, accounting for 38% of the volume of the strongbox, ensured a steady upstream water level during the contaminant transport stage. The comparatively small tail water reservoir (9% of the strongbox volume) featured an overflow valve connected to its sidewall to maintain a constant downstream water level during the in-flight stage. The SB wall was located in the model's center and was 40 mm thick and 400 mm high. The aquifer and aquitard were situated on either side of the SB wall, with 340 and 170 mm thickness, respectively. The SB wall was inserted 60 mm into the aquitard at the bottom.

2.3 Test materials and model preparation

This study used sodium chloride (NaCl) as the contaminant because Cl^- is essentially a conservative tracer (Arulanandan et al., 1988; McKinley et al., 1998), which avoided the difficulty of achieving adsorption similitude in the experiment. The concentration of NaCl was set at 0.1 mol/L, which is close to the average concentration observed in field investigations conducted by Xu et al. (2019) at landfill sites. It should be noted that landfills contain other more harmful pollutants, such as organic matter and heavy metal ions, and they are not conservative transport. Therefore, their breakthrough behavior may differ from Cl^-, and it is necessary to conduct further transport experiments for these pollutants.

Two different types of soils were used in this test: Fujian standard sand and Wyoming bentonite. The bentonite was a thoroughly natural Na-based bentonite commercially available from Wyo-Ben, Inc., Billings, Montana, USA. Its mineral composition, determined by X-ray diffraction, comprised 12.3% quartz, 12.7% andesine, 3.6% illite, and 71.4% Na-montmorillonite. The bentonite's cation exchange capacity (CEC) was 79.93 milliequivalent per 100 g, measured by the ammonium exchange method, and its specific surface area was 80.23 m^2/g, determined by the N_2 adsorption method. Table 2 shows their physical properties, and Fig. 2 illustrates their grain size distribution curves. The aquifer consisted exclusively of Fujian

Table 2 Properties of constituent soils

Soil	C_u	C_c	e_{max}	e_{min}	L_L (%)	P_I (%)	G_s
Fujian standard sand	1.7	0.96	0.85	0.52	–	–	2.64
Wyoming bentonite	–	–	–	–	342	260	2.55

C_u is the coefficient of uniformity; C_c is the coefficient of curvature; e_{max} is the maximum void ratio; e_{min} is the minimum void ratio; L_L is the liquid limit; P_I is the plasticity index; G_s is the specific gravity of soil particle

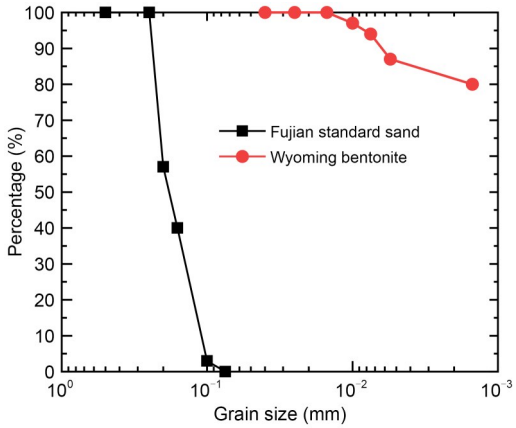

Fig. 2 Grain size distribution curve of Fujian standard sand and Wyoming bentonite

standard sand. The SB backfill and aquitard were prepared using air-dried Fujian sand, a bentonite slurry (5% bentonite in deionized water), and pure bentonite.

Before the model was prepared, four pairs of slots were fixed on the side of the strongbox for installing the perforated baffles and the SB wall construction mold. A 10-mesh screen (wire diameter 0.32 mm, aperture 2.30 mm) and filter paper were fixed on the side of the perforated baffle in contact with the soil to prevent the soil from entering the water tank. Two perforated baffles were then inserted, and a steel support frame was placed to maintain pressure equilibrium and prevent deformation of the water tank (Fig. 3a). Moreover, bentonite paste was applied to the walls of the soil storage area to inhibit water leakage between the soil and the strongbox.

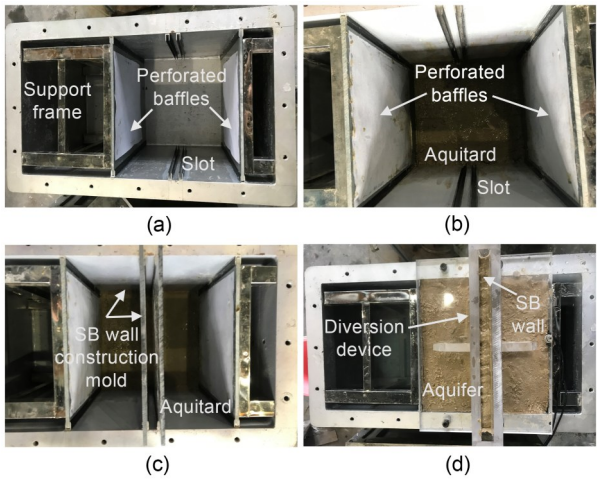

Fig. 3 Model preparation: (a) component installation; (b) aquitard preparation; (c) SB wall preparation; (d) diversion device installation

The aquitard was prepared by a moist tamping method with five lifts, each 34 mm thick, compacted using an impact compactor plate with a surface area of 0.02 m^2 and a mass of 5 kg to achieve the desired density of 1.78 g/cm^3 (Fig. 3b).

Before installing the wall model, the SB wall construction mold with a thickness of 8 mm was inserted into the slots (Fig. 3c). Then, a 6 cm aquitard was prepared on the outer side of the SB wall construction mold to form the key. To avoid trapping air bubbles, a piping bag filled with the SB backfill was used to extrude the SB backfill from the bottom of the narrow molds while being lifted gradually. Note that this differed from field construction, in which the SB backfill is placed on a slope and displaces slurry.

The same method was used to prepare the aquifer on both sides of the SB wall with a controlled density of 1.94 g/cm^3. After completing the aquifer, the SB wall construction mold was slowly pulled out of the model. The space previously occupied by the SB wall construction mold was then filled by the sinking of the SB backfill. Finally, a diversion device was installed on the top of the strongbox to supplement SB backfill during the consolidation of the SB wall (Fig. 3d). Detailed information on the diversion device can be found in Section S1 of the electronic supplementary materials (ESM). Table 3 shows the mixing proportions and physical properties of the soils after preparation.

Table 3 Mixing proportions and physical properties of the different soils after preparation

Soil	Mass fraction (%)			h_s	e_0	ρ_0
	Sand	Bentonite	Water	(mm)		(g/cm^3)
SB backfill	68.84	3.62	27.54	125	1.22	1.73
Aquifer	90.91	0	9.09	–	0.74	1.94
Aquitard	66.66	16.67	16.67	–	1.08	1.78

h_s is the slump; e_0 is the initial void ratio; ρ_0 is the initial density

2.4 Test materials and model preparation

In this study, four types of sensors were used: pore pressure transducer, strain-type earth pressure cell, non-contact type laser distance sensor, and differential pressure sensor. Pore pressure transducers, with an accuracy of ±1 kPa, were placed at the bottom of the head and tail water reservoirs to monitor changes in water levels. Strain-type earth pressure cells, with an accuracy of ±2 kPa, were attached to the side of

the SB wall to measure horizontal earth pressure. The method for installation of the soil pressure sensor can be found in Section S2 of the ESM. Laser sensors, with an accuracy of ±0.05 mm, were mounted above the SB wall to monitor its settlement. Additionally, a differential pressure sensor with an accuracy of ±0.04 kPa was placed in the collection device to measure the seepage discharge. Fig. 1 provides the details of the sensor installation locations during model preparation. Note that the positions of the earth pressure cells changed due to the settlement of the soil. Therefore, their positions were remeasured after the experiment.

2.5 Test procedure

The test was divided into three stages: consolidation, watertightness testing, and contaminant migration.

In the first stage, the model was centrifuged at 100*g*. The high porosity SB backfill was consolidated and supplemented with SB backfill via the diversion device. This stage lasted for over 8 h until the settlement rate of the SB wall fell below 1 mm/h, a criterion also adopted by Wang et al. (2016).

The second stage aimed to examine the watertightness between the soil and the strongbox by setting a head difference of 3.00 cm between the upstream and downstream. When the seepage discharge in the model was less than the calculated value of 27.36 mL/h, it indicated no significant leakage between the soil and the strongbox. Note that the calculated seepage discharge did not consider the preferential flow through the interface between the SB wall and the aquitard due to the unknown permeability of the interface, which differed from the actual situation. Additionally, due to the unknown hydraulic conductivity of the SB wall, this value was calculated using the upper limit of the SB wall's hydraulic conductivity (1×10^{-9} m/s). If the seepage discharge substantially exceeded the calculated value, the model had to be reprepared. This stage lasted about 3 h. In this test, the actual head difference was 3.56 cm and the average seepage discharge was 24.68 mL/h. Thus, the watertightness of the model satisfied the requirements.

Before the start of the third stage, the deionized water in the head water reservoir was replaced with a 0.1 mol/L NaCl solution to simulate the pollution source. The expected water level difference between the two reservoirs was set as 3.00 cm but measured 3.66 cm in practice, with a seepage discharge of 26.44 mL/h. This stage lasted 36 h, equivalent to 41 years of transport time in the prototype. Due to an average ambient temperature of 38 °C in the centrifuge chamber, evaporation caused a decrease in water levels in both reservoirs. However, the unit area evaporation rates of the two reservoirs were similar, maintaining a head difference of 3.66 cm. According to P2, the downstream water level was 11.48 cm below the top of the SB wall at the end of the test. Photographs of the centrifuge model are shown in Fig. S2 of the ESM.

Before sampling, a wire saw was used to cut the SB wall along the slot and the top surface of the aquitard. The extracted SB wall was placed on a flat operating platform (Fig. 4a). Three series of samples were collected from the SB wall along the height direction (Fig. 4b). The moisture content and density of the samples were determined by ASTM (2019) and ASTM (2021), respectively. Hydraulic conductivity tests were conducted with the flexible-wall permeameter using the constant head method, as per ASTM (2016). Additionally, the bottom of the embedded part of the SB wall exhibited a mud-like state, suggesting that the consolidation stress at that location was low. Consequently, the porosity and hydraulic conductivity at the bottom of the SB wall were determined using the transport parameters of the unconsolidated SB backfill. The method for testing sample concentration is detailed in Section S4 of the ESM.

3 Numerical simulation of contaminant transport for centrifuge modeling

3.1 Numerical modeling

An FE method program, COMSOL Multiphysics 5.5, was used to investigate the transport behavior of contaminants in the centrifuge test. The convection-dispersion equation was used as the governing equation in the solute transport model (Yao et al., 2023), as shown in Eq. (1):

$$\frac{\partial C_i}{\partial t}=D_{x,i}\frac{\partial^2 C_i}{\partial x^2}+D_{z,i}\frac{\partial^2 C_i}{\partial z^2}-v_{x,i}\frac{\partial C_i}{\partial x}-v_{z,i}\frac{\partial C_i}{\partial x}, \quad (1)$$

where *i* represents 'ua', 'cw', 'da', or 'at' ('ua' represents upstream aquifer, 'cw' represents SB wall, 'da'

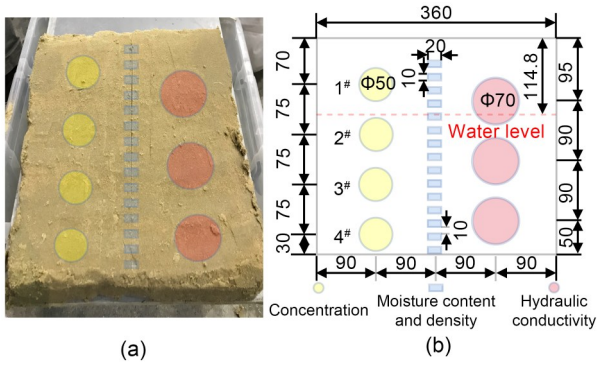

Fig. 4 Sample collection: (a) SB wall on the operating platform; (b) schematic of sampling locations (mm)

represents downstream aquifer, and 'at' represents aquitard); C_i denotes the contaminant concentration of each part; $D_{x,i}$ and $D_{z,i}$ represent the horizontal and vertical hydrodynamic dispersion coefficients, respectively; $D_{x,i}=\tau_i D_0+\alpha_i v_{x,i}$ and $D_{z,i}=\tau_i D_0+\alpha_i v_{z,i}$ (τ_i is the tortuosity factor, $\tau_i=n_i^{1/3}$ (Mott and Weber, 1991); n_i is the porosity of different soil; D_0 is the aqueous molecular diffusion coefficient; α_i is the dispersivity); $v_{x,i}$ and $v_{z,i}$ are the horizontal and vertical seepage velocities, respectively.

A two-dimensional (2D) FE model corresponding to the dimensions of centrifuge modeling was established (Fig. 5). It is important to emphasize that the numerical model used in this study was developed at the model scale rather than the prototype scale. The centrifugal acceleration g_c in the numerical model was set to 100g. The increase in g_c induced a greater pore water pressure gradient, leading to a heightened seepage velocity v and an increased hydrodynamic dispersion coefficient. This is the effect of g_c on the pollutant transport governing equation.

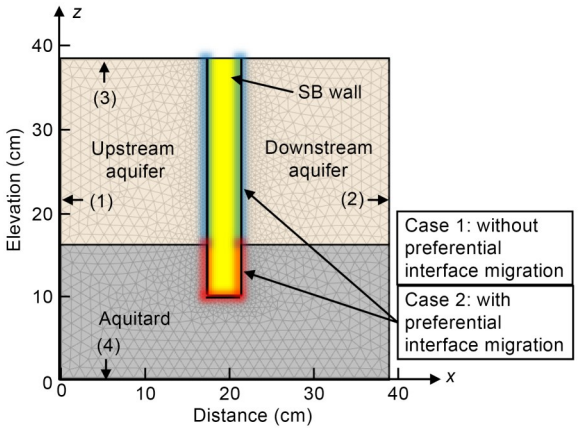

Fig. 5 Two-dimensional FE model of centrifuge test: mesh and boundary conditions. (1)–(4) represent boundaries

The concentration of sample 1#, located above the water level in the experiment, was nearly 0 (Fig. 4b). This suggests that the contaminant transport in the unsaturated zone was notably slow. Therefore, for modeling simplicity, the simulation was confined to the saturated zone (its height and length are 38.16 cm and 39.00 cm respectively, as shown in Fig. 5). Four boundaries are outlined in the equations shown in Table 4: the inflow boundary, outflow boundary, upper boundary, and lower boundary. The layer interface should comply with the continuity conditions of concentration, contaminant flux, pressure, and seepage flux. The numerical model used a constant head difference h_w of 3.66 cm and a constant Cl^- concentration of the head water reservoir C_0 of 0.1 mol/L. This numerical model is referred to as case 1.

Table 4 Boundary conditions of model

Boundary	Type	Contaminant transport	Seepage
(1)	Inflow boundary	$C=C_0$	$P=\rho_f g_c(H_m-z+h_w)$
(2)	Outflow boundary	$\frac{\partial C}{\partial x}=0$	$P=\rho_f g_c(H_m-z)$
(3)	Upper boundary	$\frac{\partial C}{\partial z}=0$	$\frac{\partial P}{\partial z}=\rho_f g_c$
(4)	Lower boundary	$\frac{\partial C}{\partial z}=0$	$\frac{\partial P}{\partial z}=\rho_f g_c$

P is the pore water pressure; H_m is the model height; ρ_f=993 kg/m^3 (38 ℃); z is the elevation of the numerical model

Notably, the results of case 1 on the contaminant distribution differed significantly from those of the centrifuge test (Fig. 8 in Section 4.3). The contaminant concentration within the SB wall was higher downstream than in the middle, and deeper regions exhibited a greater concentration than shallower ones. This concentration distribution indicated that pollutants did not reach the downstream aquifer via the SB wall; instead, they migrated directly from the interface between the SB wall and the aquitard, circumventing the base of the SB wall to reach the downstream aquifer. To validate this hypothesis, a small-scale dye tracing experiment under the condition of 1g using a transparent box was performed. The soil materials and preparation methods for this experiment were consistent with the centrifuge test. The results revealed that the red dye bypassed the base of the SB wall and swiftly reached the downstream aquifer (detailed information on this test can be found in Section S5 of the ESM).

When the SB wall and aquitard in the experiment were without defects, the interface between them was likely to become the pathway with the lowest resistance to water and pollutant transport. In particular, the length of the key of the SB wall was scaled down in centrifuge tests, which means that the hydraulic path between the interfaces was also shortened relative to the field condition, resulting in a more significant preferential interface migration. Additionally, the base soil of the SB mixture used in the experiment (Fujian standard sand) had a larger particle size, making the interface between the SB wall and aquitard rougher, which further promoted the generation of preferential interface migration. In subsequent studies, silt with a smaller particle size was used as the base soil of the SB mixture for centrifuge tests. The preferential interface migration then essentially disappeared when maintaining the same experimental setup, model preparation, and test procedure. Therefore, in practical engineering, when the in-situ soil has a larger particle size, such as sand, it cannot be directly used as the base soil for SB backfill. Instead, smaller particle-size silt or clay should be used as the base soil for SB backfill to prevent the generation of preferential interface migration.

To simulate preferential interface migration, Rowe and AbdelRazek (2019) introduced a transmissive layer with a high hydraulic conductivity into the numerical model. Inspired by this, we introduced transmissive layers to simulate preferential interface migration. However, the finite elements were proved inadequate for calculating its effect due to the layer's extremely fine spacing compared to the model components. To address this, we adopted the approach of Mozafari et al. (2018) using "fractures" to simulate preferential interface migration. Within COMSOL Multiphysics® software, fractures are not represented as physical entities but are simplified as internal boundaries, offering an effective solution to multi-scale challenges. The governing equation of contaminant transport and water flow in a fracture can be found in Section S6 of the ESM.

Therefore, this study adopted the internal boundaries of fractures to simulate preferential interface migration. In the numerical model of case 2, the internal boundaries of fractures were added at the interface between the SB wall and the surrounding soil. Briefly, this study involved two numerical models, case 1 without preferential interface migration and case 2 with preferential interface migration, to simulate Cl^- transport in the centrifuge test.

3.2 Parameters in the numerical model

The numerical simulation requires two sets of input parameters:

Transport parameters of each soil, used in the two numerical models (case 1 and case 2), are shown in Table 5 and Fig. 6. The porosity n_i and hydraulic conductivity k_i of each soil were determined through after-test sampling results. Notably, the parameters of the aquifer and aquitard were set as constant, considering their negligible change with depth. The dispersivity α_i of soils was found by reference to Gelhar et al. (1992) and Wang et al. (2016). The aqueous molecular diffusion coefficient D_0 of Cl^- was obtained from the transport parameter manual (Yaws, 2014).

Table 5 Transport parameters in the numerical model

Soil	n_i	k_i (m/s)	D_0 (m²/s)	α_i (m)
Aquifer	0.36	2.1×10^{-5}	2.78×10^{-9} [a]	0.5 [b]
SB wall	$n_{cw}(z)$	$k_{cw}(z)$	2.78×10^{-9} [a]	0.0068 [c]
Aquitard	0.49	1×10^{-12}	2.78×10^{-9} [a]	0.0068 [c]

Data were measured and calculated in this study except the following: a. Yaws (2014); b. Gelhar et al. (1992); c. Wang et al. (2016)

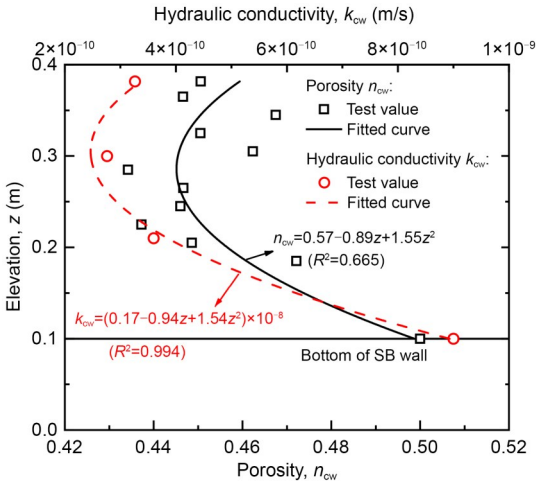

Fig. 6 Hydraulic conductivity and porosity of the SB wall in the numerical model

Transport parameters of each fracture were used only in case 2 (Table 6). The pore diameter d_f of each fracture was determined by fitting the seepage discharge (26.44 mL/h) measured during the contaminant transport phase. The porosity n_f of different fractures

Table 6 Transport parameters of each fracture

Type of fracture	d_f (mm)	n_f	$D_{0,f}$ (m²/s)	α_f (m)
SB wall-aquifer	0.0480	1	2.78×10^{-9}	3
SB wall-aquitard	0.0076	1	2.78×10^{-9}	1

was taken as 1, referring to Zhan et al. (2023b). The aqueous molecular diffusion coefficient $D_{0,f}$ of different fractures was the same as in Table 5. The dispersivity α_f of different fractures was obtained by fitting the concentration distribution of contaminants.

4 Results and discussion

4.1 Horizontal effective stress

Fig. 7 shows the normalized horizontal effective stress σ_h'/H (σ_h' is the horizontal effective stress; H is the height of the SB wall) of the SB wall from this and other published studies, and the detailed information on these SB walls is presented in Table 7. Notably, the dimensions of the SB wall in this study were converted to a prototype scale. The horizontal effective stress of the SB wall in this study showed an initial increase and a subsequent decrease with depth,

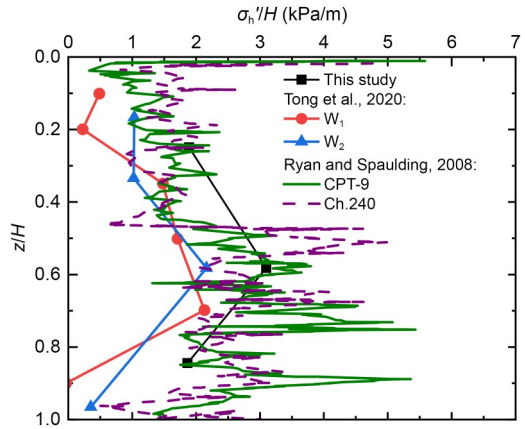

Fig. 7 Comparison of results from different studies of horizontal effective stress in an SB wall after normalization

which was consistent with some field measurements (Ryan and Spaulding, 2008; Tong et al., 2020). This horizontal stress distribution can be attributed to arching and lateral squeezing effects during the consolidation of the SB wall (Ruffing et al., 2010; Li et al., 2015; Ke et al., 2018). In contrast, Zhan et al. (2023a) conducted a centrifuge model test using rigid porous stones to support an SB wall. This method prevented the inward movement of the trench side walls, resulting in little variation in wall stress with depth. Furthermore, the σ_h'/H in this study exceeded that measured by Tong et al. (2020) but was consistent with the findings of Ryan and Spaulding (2008). This disparity may be attributable to the differences in the base soil of the SB wall.

The stress state of SB backfills significantly impacts the transport parameters of SB walls, such as porosity and hydraulic conductivity (Filz et al., 2001; Yeo et al., 2005). Therefore, it is crucial to ensure the similarity between the stress states of SB walls in both centrifuge models and prototypes for the accurate simulation of pollutant transport.

4.2 Similitude of contaminant transport

The similitude of π_2 and π_8 are discussed in this section.

$$\pi_2=\frac{\rho_f v_s l_p}{\mu}, \tag{2}$$

where ρ_f=993 kg/m³; $v_s=Q/(An_{cw})$, in which Q is the seepage discharge, Q=26.44 mL/h, A is the flow area of the SB wall, A=756.72 cm², and n_{cw} is the porosity of the SB wall. Considering the variation of porosity with depth, the average value was taken: n_{cw}=0.45, l_p=0.14 mm, and $\mu=0.68\times10^{-3}$ Pa·s.

$$\pi_8=\frac{v_s l_p}{D_m}, \tag{3}$$

Table 7 Comparison of SB walls in this and other published studies

SB wall	H (m)	b (m)	B_c (%)	Base soil	Measuring method	Reference
This study	38.5	4.0	5.0	Sand	Earth pressure cells	
W_1	6.0	0.6	4.7	Silty clay	Earth pressure cells	Tong et al. (2020)
W_2	10.0	0.6	4.7	Silty clay	Earth pressure cells	Tong et al. (2020)
CPT-9	35.0	0.8	–	Sand	CPTU	Ryan and Spaulding (2008)
Ch.240	30.0	0.8	–	Sand	CPTU	Ryan and Spaulding (2008)

b is the thickness of the SB wall; B_c is the bentonite content. The method for converting piezocone penetration test (CPTU) results to effective horizontal stress is given by Ke et al. (2018)

where $D_m=\tau_{cw}D_0$, in which τ_{cw} is the tortuosity factor of the SB wall, $\tau_{cw}=n_{cw}^{1/3}$ (Mott and Weber, 1991; Li et al., 2022); D_0=2.78×10^{-9} m^2/s.

The π_2 and π_8 were calculated as 4.42×10^{-5} and 0.011, respectively. As they were less than 1, they met the similarity requirement.

4.3 Migration behavior of chloride ions through the SB barrier system

Fig. 8 illustrates the distribution of Cl^- concentration across the thickness of the SB wall, obtained from the after-test sampling results after 36 h transport (scattered points) and simulated outcomes from case 1 and case 2. The horizontal *X*-axis represents the SB wall thickness L_{cw}, where L_{cw}=0 denotes the location of contact between the SB wall and the upstream aquifer. The longitudinal *Y*-axis shows the relative Cl^- concentration C_{cw}/C_0.

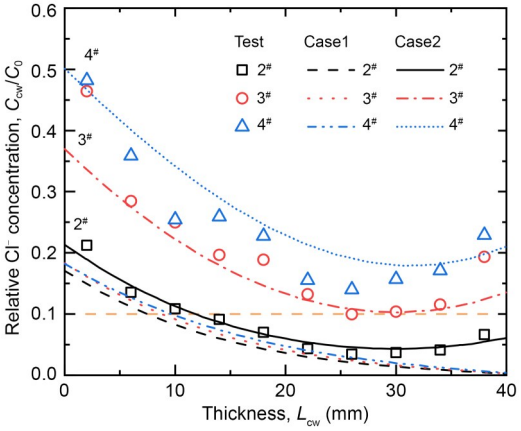

Fig. 8 Cl^- concentration distribution of simulation and test

The Cl^- concentration across the SB wall increased progressively with depth according to the test results. Near the inlet of the SB wall, the C_{cw}/C_0 at depths 2#, 3#, and 4# were 0.21, 0.46, and 0.48, respectively, while at the outlet, the values were 0.067, 0.190, and 0.230. Given the threshold for a breakthrough at the outlet, C_{cw}/C_0=0.1, as Zeng et al. (2022) noted, the deeper part of the SB wall (3# and 4#) breached the threshold after 36 h. Hence, the lower part of the SB wall was considered the weakest part of the vertical barrier, requiring measures to improve performance. However, the Cl^- concentration along with the thickness direction of the SB wall at each depth decreased initially and then increased. This distribution diverged from the results of analytical solutions based on the convection-diffusion governing equation, which anticipates a decline in pollutant concentration as the distance from the pollution source increases (Acar and Haider, 1990; Rubin and Rabideau, 2000; Li et al., 2017).

The simulation results showed a significant difference between case 1, which did not consider preferential interface migration. Specifically, case 1 exhibited much smaller Cl^- concentrations and did not increase in the thickness direction. In contrast, case 2, which considered preferential interface migration, closely resembled the centrifuge test results. In the experiment, Cl^- rapidly migrated along the interface between the SB wall and the aquitard, passing through the bottom of the SB wall and reaching the downstream aquifer, resulting in a higher concentration at the outlet of the SB wall than that in the middle. This accounts for the concentration distribution of pollutants inside the SB wall in Fig. 8. The discovery warrants scrutiny, as preferential pathways in the field-constructed wall would represent a significant defect, potentially seriously reducing the performance of the SB wall.

Fig. 9 shows the simulation results of the Cl^- contaminant plume in case 2 at different times, with the green line denoting the C_i/C_0=0.1 contour. Within the vertical barrier system, preferential pathways at the interface between the SB wall and the aquitard resulted in a seepage velocity at the base of the aquifer which exceeded that in its shallower regions. This phenomenon led to rapid migration of Cl^- downstream from the bottom of the aquifer. After 5.2 h, the Cl^- concentration front reached the SB wall and rapidly transported along the aquitard-SB wall interface. By 13.8 h, the Cl^- concentration front reached the downstream aquifer at point *B*. At 26.2 h, the Cl^- concentration front reached the tailwater reservoir, and "U"-shaped contaminant plumes emerged in the SB wall.

Based on numerical simulation, the Cl^- breakthrough point of the SB barrier system occurred at the junction (point *B*) where the SB wall, aquitard, and downstream aquifer intersect. The breakthrough time of the SB barrier system was 13.8 h, which equated to 15.75 years in the prototype. Notably, the breakthrough time was only about 1/9 of that without preferential interface migration (118.2 h).

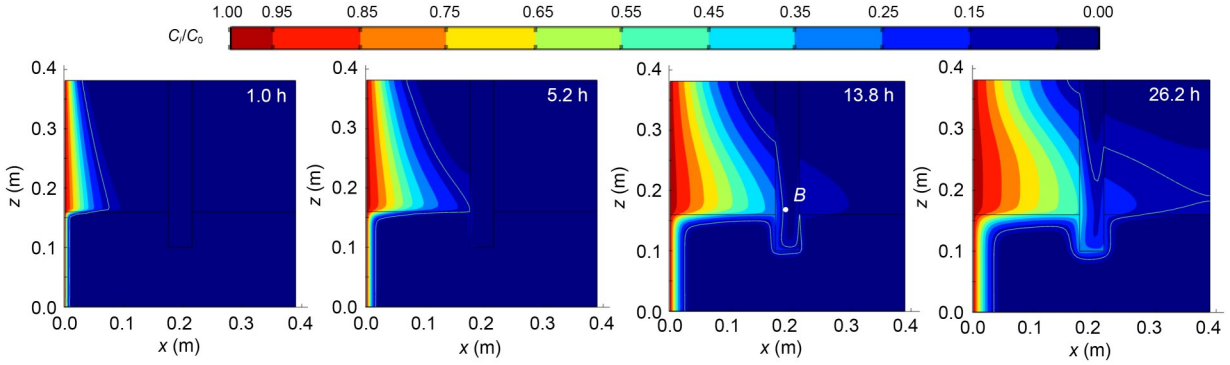

Fig. 9 Numerical simulation results for the Cl^- contaminant plume in the model at different times (C_i/C_0). References to color refer to the online version of this figure

5 Conclusions

Based on the centrifuge modeling test and numerical simulations, the following conclusions were drawn:

(1) The horizontal effective stress of the SB wall in the centrifuge modeling showed an initial increase and then a decrease with depth, which is consistent with some field measurements. The similarity in stress states ensured that the transport parameters (such as porosity and hydraulic conductivity) of the SB wall and the contact state between the SB wall and its surrounding soil were consistent with the prototype.

(2) In the vertical SB barrier system, preferential interface migration occurred and significantly affected the migration behavior of contaminants. The contaminants migrated rapidly along the interface of the SB wall and aquitard, bypassing the bottom of the SB wall and reaching downstream. This observation differed from the traditional migration pathway. The preferential interface migration, as a defect, greatly accelerated the migration speed of contaminants, reducing the breakthrough time of the SB wall to about 1/9 of that without preferential interface migration, which deserves attention in practical applications.

(3) An internal boundary called a "fracture" was used in the numerical model to simulate the preferential interface migration. The simulation results agreed with those from the centrifuge test, affirming the viability of this simulation approach.

(4) The base soil of the SB wall used in the experiment (Fujian standard sand) had a larger particle size, making the interface between the SB wall and aquitard rougher, which promoted the generation of preferential interface migration. Therefore, in practical engineering, when the in-situ soil is sand with a larger particle size, it cannot be directly used as the base soil for an SB wall. Instead, smaller particle-size silt or clay should be used to serve as the base soil for SB backfill to prevent the generation of preferential interface migration.

Acknowledgments

This work is supported by the National Key Research and Development Program of China (No. 2018YFC1802304), the National Natural Science Foundation of China (Nos. 51988101 and 42077241), and the Natural Science Foundation of Zhejiang Province (No. LCZ19E080002), China.

Author contributions

Yuchao LI designed the research. Linfeng CAO processed the corresponding data and wrote the first draft of the manuscript. Jiachen GUO and Chunrui XU helped to organize the manuscript. Bo HUANG revised and edited the final version.

Conflict of interest

The authors declare that they have no known competing financial interests or personal relationships that could have appeared to influence the work reported in this paper.

References

Acar YB, Haider L, 1990. Transport of low-concentration contaminants in saturated earthen barriers. *Journal of Geotechnical Engineering*, 116(7):1031-1052. https://doi.org/10.1061/(ASCE)0733-9410(1990)116:7(1031)

Arulanandan K, Thompson PY, Kutter BL, et al., 1988. Centrifuge modeling of transport processes for pollutants in soils. *Journal of Geotechnical Engineering*, 114(2):185-205. https://doi.org/10.1061/(ASCE)0733-9410(1988)114:2(185)

ASTM (American Society for Testing and Materials), 2016.

Standard Test Methods for Measurement of Hydraulic Conductivity of Saturated Porous Materials Using a Flexible Wall Permeameter, ASTM D5084-16a. ASTM, West Conshohocken, PA, USA. https://doi.org/10.1520/D5084-16A

ASTM (American Society for Testing and Materials), 2019. Standard Test Methods for Laboratory Determination of Water (Moisture) Content of Soil and Rock by Mass, ASTM D2216-19. ASTM, West Conshohocken, PA, USA. https://doi.org/10.1520/D2216-19

ASTM (American Society for Testing and Materials), 2021. Standard Test Methods for Laboratory Determination of Density and Unit Weight of Soil Specimens, ASTM D7263-21. ASTM, West Conshohocken, PA, USA. https://doi.org/10.1520/D7263-21

Cao BY, Xu J, Wang F, et al., 2021. Vertical barriers for land contamination containment: a review. *International Journal of Environmental Research and Public Health*, 18(23): 12643. https://doi.org/10.3390/ijerph182312643

Cooke B, Mitchell RJ, 1991. Physical modelling of a dissolved contaminant in an unsaturated sand. *Canadian Geotechnical Journal*, 28(6):829-833. https://doi.org/10.1139/t91-100

D'appolonia DJ, 1980. Soil-bentonite slurry trench cutoffs. *Journal of the Geotechnical Engineering Division*, 106(4): 399-417. https://doi.org/10.1061/AJGEB6.0000945

Filz GM, Henry LB, Heslin GM, et al., 2001. Determining hydraulic conductivity of soil-bentonite using the API filter press. *Geotechnical Testing Journal*, 24(1):61-71. https://doi.org/10.1520/GTJ11282J

Gamerdinger AP, Kaplan DI, Wellman DM, et al., 2001. Two-region flow and decreased sorption of uranium (VI) during transport in hanford groundwater and unsaturated sands. *Water Resources Research*, 37(12):3155-3162. https://doi.org/10.1029/2001WR000247

Gelhar LW, Welty C, Rehfeldt KR, 1992. A critical review of data on field-scale dispersion in aquifers. *Water Resources Research*, 28(7):1955-1974. https://doi.org/10.1029/92WR00607

Hensley PJ, Schofield AN, 1991. Accelerated physical modelling of hazardous-waste transport. *Géotechnique*, 41(3): 447-465. https://doi.org/10.1680/geot.1991.41.3.447

Hutchison JM, Seaman JC, Aburime SA, et al., 2003. Chromate transport and retention in variably saturated soil columns. *Vadose Zone Journal*, 2(4):702-714. https://doi.org/10.2136/vzj2003.7020

Ke H, Tong X, Li YC, et al., 2018. Force equilibrium-based model for predicting stresses in soil-bentonite cutoff walls. *Journal of Geotechnical and Geoenvironmental Engineering*, 144(2):04017112. https://doi.org/10.1061/(ASCE)GT.1943-5606.0001821

Kererat C, Sasanakul I, Soralump S, 2013. Centrifuge modeling of LNAPL infiltration in granular soil with containment. *Journal of Geotechnical and Geoenvironmental Engineering*, 139(6):892-902. https://doi.org/10.1061/(ASCE)GT.1943-5606.0000754

Knight MA, Mitchell RJ, 1996. Modelling of light nonaqueous phase liquid (LNAPL) releases into unsaturated sand. *Canadian Geotechnical Journal*, 33(6):913-925. https://doi.org/10.1139/t96-121

Kumar RP, Singh DN, 2012. Geotechnical centrifuge modeling of chloride diffusion through soils. *International Journal of Geomechanics*, 12(3):327-332. https://doi.org/10.1061/(ASCE)GM.1943-5622.0000139

Lee T, Benson CH, 2000. Flow past bench-scale vertical groundwater cutoff walls. *Journal of Geotechnical and Geoenvironmental Engineering*, 126(6):511-520. https://doi.org/10.1061/(ASCE)1090-0241(2000)126:6(511)

Li JS, Jiang WH, Ge SQ, et al., 2022. Coupled model for consolidation and organic contaminant transport in GMB/CCL composite liner under non-isothermal distribution condition. *Computers and Geotechnics*, 150:104893. https://doi.org/10.1016/j.compgeo.2022.104893

Li YC, Cleall PJ, Wen YD, et al., 2015. Stresses in soil-bentonite slurry trench cut-off walls. *Géotechnique*, 65(10): 843-850. https://doi.org/10.1680/jgeot.14.P.219

Li YC, Chen GN, Chen YM, et al., 2017. Design charts for contaminant transport through slurry trench cutoff walls. *Journal of Environmental Engineering*, 143(9):06017005. https://doi.org/10.1061/%28ASCE%29EE.1943-7870.0001253

Lo IMC, Zhang JH, Hu LM, 2005. Centrifuge modeling of cadmium migration in saturated and unsaturated soils. *Soil and Sediment Contamination: an International Journal*, 14(5):417-431. https://doi.org/10.1080/15320380500180440

McKinley JD, Price BA, Lynch RJ, et al., 1998. Centrifuge modelling of the transport of a pulse of two contaminants through a clay layer. *Géotechnique*, 48(3):421-425. https://doi.org/10.1680/geot.1998.48.3.421

Mott HV, Weber WJ, 1991. Diffusion of organic contaminants through soilbentonite cutoff barriers. *Research Journal of the Water Pollution Control Federation*, 63(2):166-176.

Mozafari B, Fahs M, Ataie-Ashtiani B, et al., 2018. On the use of COMSOL multiphysics for seawater intrusion in fractured coastal aquifers. *E3S Web of Conferences*, 54: 00020. https://doi.org/10.1051/e3sconf/20185400020

Rowe RK, Abdelrazek AY, 2019. Effect of interface transmissivity and hydraulic conductivity on contaminant migration through composite liners with wrinkles or failed seams. *Canadian Geotechnical Journal*, 56(11):1650-1667. https://doi.org/10.1139/cgj-2018-0660

Rubin H, Rabideau AJ, 2000. Approximate evaluation of contaminant transport through vertical barriers. *Journal of Contaminant Hydrology*, 40(4):311-333. https://doi.org/10.1016/S0169-7722(99)00060-1

Ruffing D, Evans J, Coughenour N, 2018. Soil-bentonite slurry trench cutoff wall longevity. IFCEE 2018, p.214-223. https://doi.org/10.1061/9780784481608.021

Ruffing DG, Evans JC, Malusis MA, 2010. Prediction of earth pressures in soil-bentonite cutoff walls. GeoFlorida

2010: Advances in Analysis, Modeling & Design, p.2416-2425.
https://doi.org/10.1061/41095(365)245

Ryan C, Ruffing D, Evans JC, 2022. Soil bentonite slurry trench cutoff walls: history, design, and construction practices. Geo-Congress 2022, p.89-99.
https://doi.org/10.1061/9780784484050.010

Ryan CR, Spaulding CA, 2008. Strength and permeability of a deep soil bentonite slurry wall. GeoCongress 2008: Geotechnics of Waste Management and Remediation, p.644-651.
https://doi.org/10.1061/40970(309)81

Shu S, Zhu W, Wang SW, et al., 2018. Leachate breakthrough mechanism and key pollutant indicator of municipal solid waste landfill barrier systems: centrifuge and numerical modeling approach. *Science of the Total Environment*, 612:1123-1131.
https:// doi.org/10.1016/j.scitotenv.2017.08.185

Soga K, Kawabata J, Kechavarzi C, et al., 2003. Centrifuge modeling of nonaqueous phase liquid movement and entrapment in unsaturated layered soils. *Journal of Geotechnical and Geoenvironmental Engineering*, 129(2):173-182.
https://doi.org/10.1061/(ASCE)1090-0241(2003)129:2(173)

Tachavises C, Benson CH, 1997. Hydraulic importance of defects in vertical groundwater cut-off walls. Proceedings of the Conference on In Situ Remediation of the Geoenvironment, p.168-180.

Timms W, Hendry MJ, Muise J, et al., 2009. Coupling centrifuge modeling and laser ablation inductively coupled plasma mass spectrometry to determine contaminant retardation in clays. *Environmental Science & Technology*, 43(4):1153-1159.
https://doi.org/10.1021/es8020414

Tong X, Li YC, Ke H, et al., 2020. In situ stress states and lateral deformations of soil-bentonite cutoff walls during consolidation process. *Canadian Geotechnical Journal*, 57(1):139-148.
https://doi.org/10.1139/cgj-2018-0503

Wang YZ, Chen YM, Xie HJ, et al., 2016. Lead adsorption and transport in loess-amended soil-bentonite cut-off wall. *Engineering Geology*, 215:69-80.
https://doi.org/10.1016/j.enggeo.2016.11.002

Wei SJ, Li YC, Shen P, et al., 2023. Molecular force mechanism of hydrodynamics in clay nanopores. *Journal of Zhejiang University-SCIENCE A (Applied physics & Engineering)*, 24(9):817-827.
https://doi.org/10.1631/jzus.A2200427

Xu HQ, Shu S, Wang SW, et al., 2019. Studies on the chemical compatibility of soil-bentonite cut-off walls for landfills. *Journal of Environmental Management*, 237:155-162.
https://doi.org/10.1016/j.jenvman.2019.02.051

Yao SY, Li YC, Tong S, et al., 2023. Numerical investigation of the effect of geosynthetic clay liner chemical incompatibility on flow and contaminant transport through a defective composite liner. *Journal of Zhejiang University-SCIENCE A (Applied physics & Engineering)*, 24(7):557-568.
https://doi.org/10.1631/jzus.A2200416

Yaws CL, 2014. Diffusion coefficient at infinite dilution in water–inorganic compounds. *In*: Transport Properties of Chemicals and Hydrocarbons. Gulf Professional Publishing, Houston, Texas, USA, p.704-705.

Yeo SS, Shackelford CD, Evans JC, 2005. Consolidation and hydraulic conductivity of nine model soil-bentonite backfills. *Journal of Geotechnical and Geoenvironmental Engineering*, 131(10):1189-1198.
https://doi.org/10.1061/(ASCE)1090-0241(2005)131:10(1189)

Zeng X, Su J, Wang HY, et al., 2022. Centrifuge modeling of chloride ions completely breakthrough kaolin clay liner. *Sustainability*, 14(12):6976.
https://doi.org/10.3390/su14126976

Zhan LT, You YQ, Zhao R, et al., 2023a. Centrifuge modelling of lead retardation in soil-bentonite cut-off walls. *International Journal of Physical Modelling in Geotechnics*, 23(4):166-179.
https://doi.org/10.1680/jphmg.21.00007

Zhan LT, Cao LF, Zhao R, et al., 2023b. Performances of the soil-bentonite cutoff wall composited with geosynthetic clay liners: large-scale model tests and numerical simulations. *Sustainability*, 15(3):1886.
https://doi.org/10.3390/su15031886

Electronic supplementary materials

Sections S1–S6, Figs. S1–S4